International Journal on Science and Technology (IJSAT)
E-ISSN: 2229-7677 ● Website: www.ijsat.org ● Email: editor@ijsat.org

Development of a Smart Highway Median Integrated Spiral Wind Turbine with Vehicle-Induced Airflow Enhancement

S. Kumarappa

Department of Mechanical Engineering, Bapuji Institute of Engineering and Technology, Davangere, Karnataka, India.

Abstract
The increasing demand for sustainable energy and the need to reduce the energy consumption of highway infrastructure had created opportunities for harvesting renewable energy from otherwise unused airflow sources. This study presented a Smart Highway Median with an Integrated Spiral Wind Turbine designed to utilize both ambient wind and airflow generated by moving vehicles for decentralized power generation. A three-dimensional spiral vertical-axis wind turbine was developed and evaluated using computational fluid dynamics (CFD). The numerical analysis was performed using ANSYS Fluent under steady turbulent-flow conditions with the SST k–ω turbulence model**.** The aerodynamic behaviour was investigated in terms of velocity distribution, pressure coefficient, streamlines, turbulence intensity, torque, and power coefficient at a reference wind velocity of 6 m/s. The CFD results showed significant flow acceleration around the spiral blades and a distinct downstream wake, confirming effective extraction of kinetic energy from the airflow. The pressure difference between the windward and leeward surfaces generated the aerodynamic torque required for rotor rotation. The turbine exhibited an optimum operating condition at a tip-speed ratio (TSR) of 6**,** with a maximum predicted power coefficient (Cp) of approximately 0.54. Experimental evaluation of rotor speed, torque, electrical power, and power coefficient was conducted for validation, with differences from the CFD results attributed to mechanical friction, generator losses, manufacturing tolerances, and unsteady airflow conditions. The system demonstrated promising potential for powering low-energy highway applications such as LED lighting, traffic sensors, warning indicators, and IoT-based monitoring systems**.** The integration of spiral wind turbines into highway medians provided a compact renewable-energy solution capable of converting vehicle-induced and ambient airflow into useful electrical energy.

Keywords: Smart highway, spiral vertical-axis wind turbine, CFD, vehicle-induced airflow, renewable energy.

1. Introduction

The rapid growth of road transportation, urbanization and infrastructure development has resulted in a continuous increase in energy demand. Highway infrastructure requires electricity for applications such as street lighting, traffic signals, warning systems, surveillance cameras, environmental sensors, communication equipment and other intelligent transportation systems. Conventionally, these electrical requirements are supplied through the utility grid, resulting in additional energy consumption and transmission losses. The integration of renewable-energy technologies directly into highway infrastructure provides an opportunity to generate electricity locally while reducing dependence on conventional energy sources.

Wind energy is one of the most promising renewable-energy resources because it is clean, sustainable and widely available. Conventional wind turbines are generally installed in open areas where sufficient and relatively uniform wind speeds are available. However, their integration into densely developed urban and transportation environments is often restricted by land requirements, visual impact, noise and highly variable wind conditions. These limitations have encouraged the development of compact wind-energy systems capable of operating under low-speed, turbulent and multidirectional airflow conditions.

Highways provide a unique environment for small-scale wind-energy harvesting because the movement of vehicles continuously displaces air and produces localized airflow. The airflow generated by passing vehicles can interact with a turbine installed close to the road median, in addition to the naturally available ambient wind. Although vehicle-induced airflow is transient and varies with vehicle speed, size, traffic density and distance from the turbine, it represents an otherwise unused energy source. Capturing a portion of this energy could provide supplementary electrical power for low-power highway applications.

Vertical-axis wind turbines (VAWTs) are particularly suitable for such applications because they can accept airflow from different directions without requiring a conventional yaw mechanism. Among different VAWT configurations, curved and spiral blade arrangements can provide continuous aerodynamic interaction with the incoming airflow. A spiral rotor also offers a three-dimensional blade configuration in which different blade sections interact with the airflow at different positions along the rotor height. This characteristic can be advantageous under the non-uniform and rapidly changing airflow conditions encountered near highways.

The present work proposes a Smart Highway Median with Integrated Spiral Wind Turbine for sustainable power generation. The turbine consists of a three-dimensional spiral vertical-axis rotor. The turbine is designed to be installed within the highway median so that it can utilize both ambient wind and vehicle-induced airflow. The mechanical rotation of the turbine is transmitted through a shaft to an electrical generator, and the generated electricity can be used for LED lighting, warning indicators, traffic sensors, environmental monitoring equipment and IoT-based highway systems.

To understand the aerodynamic behaviour of the design, a three-dimensional computational fluid dynamics (CFD**)** model is developed using ANSYS Fluent. The analysis considers steady, incompressible and turbulent airflow using the SST k–ω turbulence model. The turbine performance is evaluated through velocity contours, pressure-coefficient distribution, streamlines, turbulence intensity, torque, tip-speed ratio and power coefficient. A reference wind velocity of 6 m/s is considered for the principal CFD investigation.

The CFD results provide detailed information about the interaction between the airflow and spiral blade surfaces. The velocity distribution is used to identify flow acceleration and the downstream wake, while pressure-coefficient contours are used to understand the aerodynamic loading responsible for torque generation. Streamline and turbulence-intensity distributions provide information about flow separation, vortex formation and wake development. The variation of torque and power coefficient with tip-speed ratio is subsequently used to identify the optimum operating condition of the turbine.

The numerical investigation is complemented by experimental evaluation of the prototype. Parameters such as rotor speed, torque, voltage, current, mechanical power and electrical power are considered for comparison with the CFD predictions. The comparison helps identify the influence of practical factors such as bearing friction, generator losses, surface roughness, manufacturing tolerances and unsteady airflow, which are difficult to represent completely in the numerical model.

The primary objective of this study is therefore to develop, numerically investigate and experimentally assess a spiral vertical-axis wind turbine integrated into a highway median for sustainable energy generation. The study also aims to identify the aerodynamic characteristics and optimum operating condition of the turbine and to evaluate its potential for supplying decentralized power to smart-highway applications. The approach combines renewable-energy generation with existing transportation infrastructure and provides a potential pathway toward more sustainable and energy-efficient highway systems.

2. Literature Review

Vertical-axis wind turbines (VAWTs) have gained significant attention for low-speed, turbulent and multidirectional wind applications because of their omnidirectional wind acceptance and compact installation requirements. Ahmad et al. [1] reported that airfoil profile, blade number, solidity, aspect ratio, helicity and overlap ratio strongly influence VAWT performance, while dynamic stall and wake interaction remain important challenges. Barnes et al. [2] emphasized the importance of Reynolds number, geometric scaling, mesh quality and experimental validation in VAWT investigations.

Dobrev and Massouh [3] demonstrated through CFD and PIV measurements that vortex shedding, flow separation and three-dimensional wake effects significantly influence VAWT performance. Faisal et al. [4] and Kamal et al. [7] showed that Archimedes spiral turbine performance can be improved through appropriate blade geometry, aerofoil selection and rotor configuration. Ferrari et al. [5] further demonstrated that three-dimensional CFD provides better prediction of VAWT performance than simplified two-dimensional modelling. Jang et al. [6] confirmed the usefulness of combining CFD predictions with experimental and field measurements for estimating practical electrical output.

Highway-based wind-energy harvesting has also received increasing attention. Kunkel and Hall [8] identified highway medians as potential locations for compact VAWTs because passing vehicles generate additional turbulent airflow that can be harvested. Ulus and Moldovan [12] further investigated vehicle-induced highway winds and demonstrated the potential of aerodynamic flow-management techniques to enhance turbine–vehicle airflow interaction. Nawar et al. [9] reported improved performance from variable-angle Archimedes spiral blades, while Rezaeiha et al. [10] established the importance of suitable turbulence-model selection for accurate VAWT CFD prediction.

Previous studies establish the potential of spiral and helical VAWTs for low-speed applications and confirm the importance of three-dimensional CFD combined with experimental validation. However, limited research has addressed the integrated use of a three-dimensional spiral VAWT directly within a highway median to simultaneously harvest ambient and vehicle-induced airflow. The present study therefore develops a Smart Highway Median with Integrated Spiral Wind Turbine (SHM-SWT) and evaluates its aerodynamic behaviour and electrical-energy generation through CFD and experimental investigation.

The major research gap is the limited integration of spiral VAWT technology with highway-median infrastructure, particularly under transient vehicle-induced airflow. Further investigation is required into velocity distribution, pressure variation, turbulence intensity, wake interaction, torque, power coefficient and practical electrical output.

3. Methodology

The Smart Highway Median with Integrated Spiral Wind Turbine (SHM-SWT) was investigated through an integrated approach combining computational fluid dynamics (CFD) and experimental testing. The methodology encompassed spiral-turbine modeling, aerodynamic simulation, prototype fabrication, and experimental validation.

3.1 Turbine Modeling

A three-dimensional CAD model of the spiral vertical-axis wind turbine was developed with a rotor diameter of 1030 mm and an overall height of 926 mm. The spiral configuration was specifically selected to effectively capture multidirectional ambient wind and vehicle-induced airflow generated along highway medians.

3.2 CFD Analysis

The three-dimensional turbine geometry was imported into ANSYS Fluent and surrounded by an external computational fluid domain. Numerical simulations were performed for steady, incompressible turbulent flow at a reference wind velocity of 6 m/s. The SST k–ω turbulence model was employed to accurately predict flow separation, pressure gradients, and wake development across the domain. A refined unstructured mesh was applied around the blade surfaces and near-wake regions. The aerodynamic performance was characterized in terms of velocity magnitude, pressure distribution, streamlines, turbulence intensity, torque, and power coefficient. The tip-speed ratio (λ) was defined as: $\lambda = (\omega \cdot R) / V$

The rotor power coefficient (Cp) was calculated using: $Cp = P / (0.5 \cdot \rho \cdot A \cdot V^3)$

where P is the extracted mechanical power, ρ is the air density, A is the rotor swept area, R is the rotor radius, ω is the angular velocity, and V is the free-stream wind velocity.

3.3 Experimental Investigation

A physical prototype of the spiral wind turbine was fabricated in accordance with the CFD geometry and coupled to an electrical generator via a vertical drive shaft. Experimental testing was carried out across multiple wind velocities to measure wind speed, rotor rotational speed, shaft torque, output voltage, and current. The electrical power output (Pe) was calculated as:

Pe = V·I. The corresponding mechanical power (Pm) was determined from: $P_m = T \cdot \omega$,

where T represents the measured shaft torque.

3.4 CFD–Experimental Validation

The percentage deviation between the CFD and experimental results was quantified using:

$\%Error = [(X_{CFD} - X_{EXP}) / X_{CFD}] \times 100$

The validated results demonstrate the engineering feasibility of integrating spiral vertical-axis wind turbines into highway medians to generate clean renewable power for LED roadway lighting, traffic monitoring sensors, warning systems, and IoT-based smart highway infrastructure.

3.4 Experimental setup

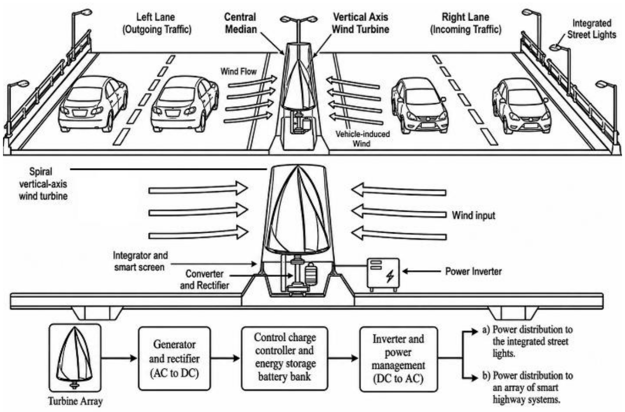

Figure 1. Schematic diagram of setup.

The Smart Highway Median with Integrated Variable-Pitch Spiral Wind Turbine was developed to utilize both vehicle-induced airflow and ambient wind for electrical power generation. The turbine was installed in the highway median to interact with airflow generated by vehicles travelling in opposite directions, along with the naturally available surrounding wind. The working principle of the system is illustrated in the corresponding figure.

The turbine consisted of a vertical-axis tapered spiral rotor with diameter of 1030 mm and a height of 926 mm**.** The rotor incorporated a tapered spiral profile in which the effective radius varied along its height. In addition, the blade pitch varied continuously along the rotor height, allowing different blade sections to interact effectively with the non-uniform airflow generated by passing vehicles. The curved spiral configuration enabled the rotor to receive airflow from different directions without requiring a yaw mechanism.

As vehicles travelled along the highway, their movement displaced the surrounding air and generated transient vehicle-induced airflow. This airflow interacted with the ambient wind and impinged on the spiral blades. The interaction produced aerodynamic lift and drag forces on the curved blade surfaces. The tangential component of these forces generated aerodynamic torque about the vertical axis. The tapered geometry enabled different sections of the rotor to interact with varying local airflow conditions, while the variable-pitch arrangement provided a favourable aerodynamic orientation along the rotor height.

The generated aerodynamic torque caused the spiral rotor to rotate about its vertical shaft. Owing to the vertical-axis configuration, the turbine was capable of receiving airflow from multiple directions without an active yawing system. Therefore, airflow generated by vehicles travelling in either direction contributed to rotor rotation. The continuous spiral configuration distributed the blade surface along the rotor height and angular position, thereby promoting relatively continuous torque generation during operation.

The rotor geometry was designed to provide sufficient starting torque under low and fluctuating wind speeds. Once the aerodynamic torque exceeded the mechanical resistance of the rotor and generator, the turbine started rotating. The rotational motion was transmitted through the vertical shaft to a permanent-magnet generator (PMG). The generator converted the mechanical energy of the rotating rotor into electrical energy. The generated electrical output was subsequently passed through a rectifier and charge controller for electrical conversion and regulation before being supplied to a battery or other energy-storage system.

The stored electrical energy was intended for LED highway lighting, warning and information boards, traffic sensors, surveillance systems, IoT-based monitoring devices, and other low-power smart-highway applications**.** The turbine is installed within the highway median, allowing multiple units to be distributed along the roadway. As vehicles continuously pass the turbine locations, the resulting airflow provides an additional source of renewable energy without requiring a separate land area. Thus, the setup converts unused vehicle-induced and ambient wind energy into useful electrical power, contributing to sustainable and self-powered highway infrastructure.

5 Results and discussions.

CFD Analysis and Discussion of the Spiral Wind Turbine

The computational fluid dynamics (CFD) analysis was carried out to investigate the aerodynamic behaviour of the Smart Highway Median with Integrated Spiral Wind Turbine. The analysis considers the three-dimensional spiral vertical-axis wind turbine operating at a reference wind velocity of 6 m/s. The simulations are performed using ANSYS Fluent under steady, incompressible and turbulent-flow conditions with the SST k–ω turbulence model. The following sections describe the CFD analysis corresponding to Figures 5.1 to 5.9.

5.1 Geometry and Computational Domain

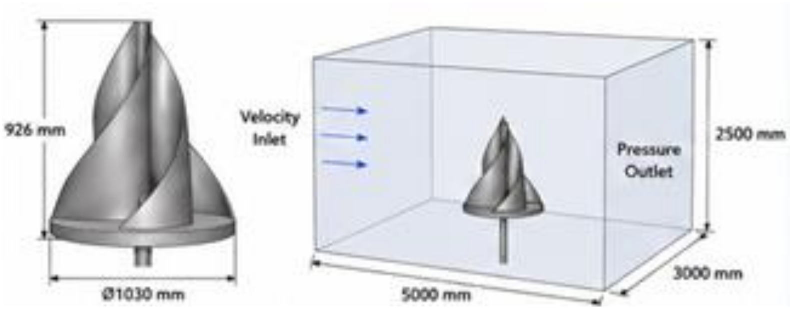

Figure 5.1 Three-dimensional geometry

Figure 5.1 presents the three-dimensional geometry of the spiral wind turbine and the computational domain used for CFD analysis. The turbine has an approximate rotor diameter of 1030 mm and a height of 926 mm. The spiral blade is positioned at the centre of the computational domain, with the airflow entering from the upstream velocity-inlet boundary and leaving through the downstream pressure-outlet boundary. The computational domain is sufficiently larger than the turbine to reduce the influence of the external boundaries on the flow around the rotor. A reference wind velocity of 6 m/s is applied at the inlet. As the airflow approaches the spiral rotor, it interacts with the curved blade surfaces and produces changes in velocity, pressure and flow direction.

The three-dimensional spiral configuration enables the turbine to receive airflow over a range of directions, making it appropriate for highway-median applications where airflow can originate from both ambient wind and the movement of vehicles. The geometry therefore forms the basic aerodynamic model for evaluating energy extraction. The geometry and domain define the physical flow problem and provide the basis for evaluating velocity distribution, pressure loading, turbulence, torque and power generation.

5.2 Mesh Distribution

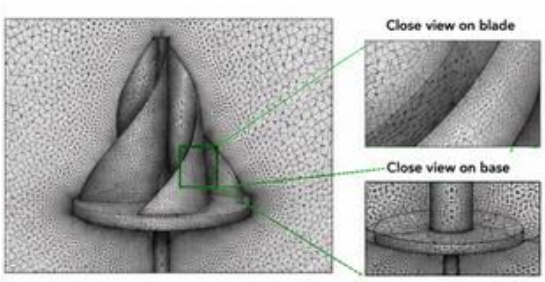

Figure 5.2 Computational mesh generated

Figure 5.2 shows the computational mesh generated around the spiral wind turbine. An unstructured tetrahedral mesh is used throughout the computational domain, with local refinement near the blade surfaces, rotor base and downstream wake region. Fine mesh elements are particularly important near the blade because the velocity and pressure gradients are high in this region. Boundary-layer refinement helps resolve the near-wall flow behaviour, while refinement in the wake region enables better prediction of vortex formation, flow separation and velocity deficit.

The mesh around the blade tip and curved spiral surfaces is also refined because these regions experience significant changes in flow direction and velocity. The resulting mesh provides sufficient spatial resolution to capture the major aerodynamic features while maintaining a practical computational requirement. Mesh refinement directly influences the accuracy of predicted aerodynamic forces and torque. A finer mesh in regions of high flow gradients improves the reliability of the velocity, pressure and turbulence results.

5.3 Velocity Magnitude Contour

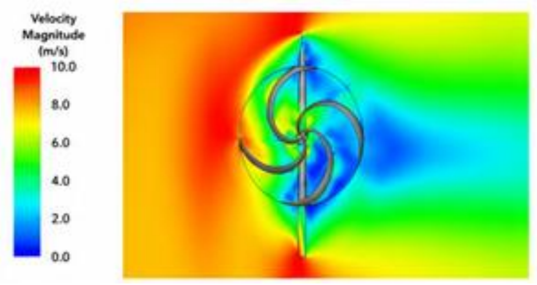

Figure 5.3 Velocity-magnitude distribution

Figure 5.3 presents the velocity-magnitude distribution around the spiral turbine at a reference inlet velocity of 6 m/s. The contour demonstrates that the airflow accelerates as it passes around the curved blade surfaces. Higher local velocities are observed around portions of the blade where the flow is constricted and redirected. A reduction in velocity is visible in the downstream region of the turbine, forming a distinct wake. This velocity deficit occurs because a portion of the kinetic energy of the incoming airflow is transferred to the rotating turbine.

The velocity distribution also indicates that the spiral blade effectively changes the direction of the incoming airflow. The continuous curvature of the blade promotes progressive flow turning and enables aerodynamic forces to act over the rotor surface. The formation of a lower-velocity wake downstream is an important indication of energy extraction. However, strong wake regions must also be considered when determining the spacing between multiple turbines installed along a highway median.

The CFD contour confirms significant velocity modification around the rotor and a clearly developed downstream wake. The velocity difference between the upstream and downstream regions demonstrates that the turbine extracts kinetic energy from the airflow. The spiral configuration provides a continuous aerodynamic interaction with the incoming wind.

5.4 Pressure Coefficient (Cp) Contour

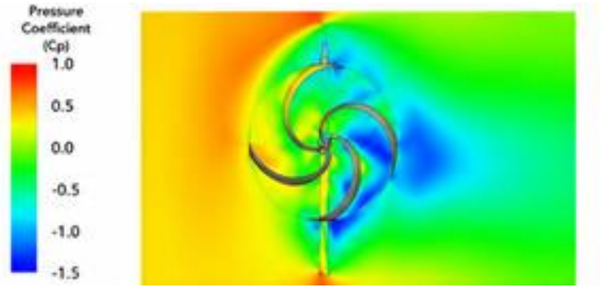

Figure 5.4 Pressure-coefficient distribution

Figure 5.4 illustrates the pressure-coefficient distribution around the spiral rotor. Higher positive pressure is observed predominantly on the windward side of the blades, whereas lower and negative pressure regions develop on the leeward side. The resulting pressure difference across the blade produces aerodynamic force. A component of this force acts in the tangential direction of the rotor and consequently generates the torque required for rotation.

The pressure distribution is not uniform along the blade because the local angle of attack and relative velocity vary continuously as the spiral blade rotates. This variation is characteristic of vertical-axis wind turbines. The low-pressure region behind and around the leeward side also contributes to the aerodynamic loading and wake development. A smooth pressure transition along the spiral surface is desirable because it reduces abrupt aerodynamic loading and helps maintain stable flow behaviour.

A clear pressure differential develops between the windward and leeward surfaces of the spiral blades. The pressure differential is the primary aerodynamic mechanism responsible for torque generation. The three-dimensional spiral geometry distributes the pressure loading over the blade surface and contributes to continuous rotational motion.

5.5 Streamline Distribution

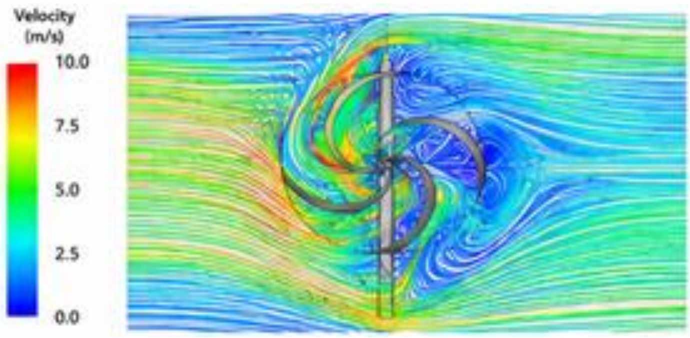

Figure 5.5 Streamline pattern

Figure 5.5 presents the streamline pattern around the spiral wind turbine. The incoming air approaches the rotor and is redirected around the curved spiral blades. The streamlines closely follow portions of the blade surface before being discharged into the downstream flow field. The figure also shows the development of vortical structures and flow recirculation in the wake. These structures are generated because the turbine removes momentum from the incoming flow and changes its direction.

The spiral geometry provides a continuous path for airflow around the blade, allowing the flow to be redirected gradually rather than undergoing an abrupt change in direction. This characteristic can help control flow separation over portions of the blade. The wake becomes more complex downstream of the rotor because of the interaction between the rotating blades and the surrounding airflow. Such wake behaviour is important for predicting the performance of multiple turbines installed in series.

The streamlines demonstrate effective airflow redirection around the spiral blade and the formation of a downstream wake containing vortical structures. The flow pattern confirms that the spiral blade interacts strongly with the incoming air and extracts momentum from the flow. Proper turbine spacing is required in a multi-turbine highway installation to avoid excessive interference between neighbouring units.

5.6 Turbulence Intensity Distribution

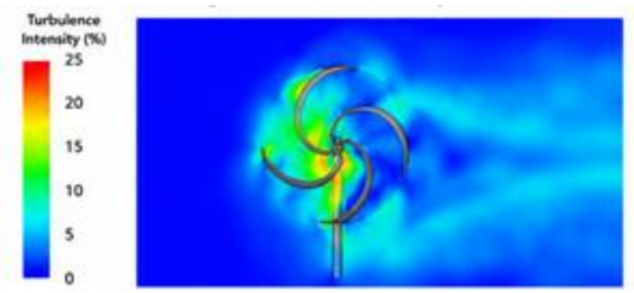

Figure 5.6 Turbulence-intensity distribution

Figure 5.6 shows the turbulence-intensity distribution around the spiral rotor. Higher turbulence intensity is concentrated near the blade surfaces, blade tips and downstream wake region. The increased turbulence near the blade is associated with strong velocity gradients, changes in flow direction and local flow separation. After the airflow passes through the rotor, the interaction of high- and low-momentum regions produces additional turbulence in the wake.

The wake turbulence gradually decreases as the distance from the turbine increases because the flow mixes with the surrounding ambient air. This behaviour indicates that the aerodynamic disturbance produced by the turbine is strongest immediately downstream of the rotor. For highway applications, turbulence analysis is particularly important because vehicle-induced airflow itself may be highly fluctuating. The CFD results can therefore assist in determining suitable turbine locations and spacing along the median.

The highest turbulence intensity occurs primarily in the blade vicinity and downstream wake, while the surrounding undisturbed region experiences relatively lower turbulence. The turbulence distribution provides information about energy losses, wake development and flow stability. Minimizing excessive separation and controlling wake interaction are important for improving turbine performance.

5.7 Pressure Distribution on Blade Surface

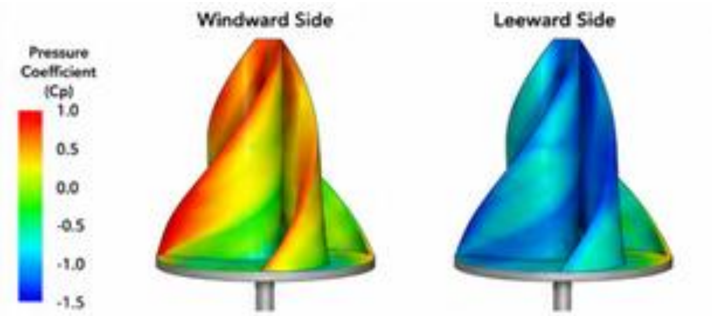

Figure 5.7 Pressure distribution over the three-dimensional spiral blade surface

Figure 5.7 presents the pressure distribution over the three-dimensional spiral blade surface. The windward surface experiences comparatively higher pressure, while the leeward surface exhibits lower pressure. This pressure difference generates the aerodynamic force acting on the blade. Because the spiral blade is curved around the vertical axis, part of this force acts tangentially and contributes directly to rotor torque.

The pressure distribution also varies along the height and curvature of the blade. This indicates that different portions of the spiral blade contribute differently to the total aerodynamic loading throughout the rotor rotation. The relatively smooth pressure variation over the spiral surface is beneficial because it avoids sudden changes in aerodynamic loading. The three-dimensional blade therefore provides a continuous aerodynamic interaction with the incoming airflow.

The windward and leeward surfaces exhibit distinct pressure levels, confirming the development of aerodynamic loading across the blade. The pressure differential is responsible for generating the aerodynamic force and rotational torque. The three-dimensional spiral geometry distributes this loading along the blade and supports continuous energy extraction.

5.8 Torque and Power Coefficient

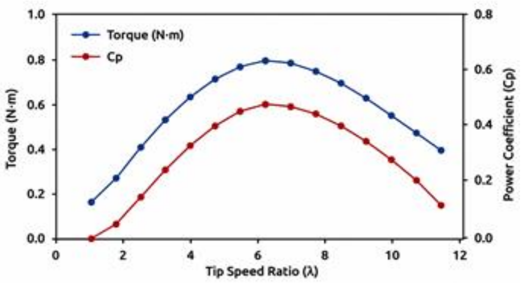

Figure. 5.8 Variation of torque and power coefficient with tip-speed ratio

Figure 5.8 presents the variation of torque and power coefficient with tip-speed ratio (TSR). Both parameters initially increase as the rotor speed increases, reach an optimum region and then decrease at higher TSR. The CFD result shown in the figure indicates a maximum power coefficient of approximately

Cp = 0.54 at TSR ≈ 6 for the investigated wind velocity of 6 m/s. This represents the optimum aerodynamic operating region of the simulated turbine.

At low TSR, the rotor rotates relatively slowly compared with the incoming airflow. Consequently, the blades cannot extract the available wind energy effectively. As TSR increases, the relative airflow over the blade improves and the aerodynamic torque and power coefficient increase. Beyond the optimum TSR, the power coefficient decreases because the blade experiences less favourable aerodynamic conditions and increased aerodynamic losses. Therefore, operation near the optimum TSR is important for maximizing energy extraction.

The power coefficient is calculated from: $Cp = P/ \{0.5 \times \rho A V^3\}$

where (P) is the extracted power, (ρ) is air density, (A) is the turbine swept area and (V) is the reference wind velocity. The simulated turbine achieves a maximum Cp of approximately 0.54 at TSR ≈ 6 under the illustrated 6 m/s operating condition. The result indicates that the spiral turbine has a defined optimum operating range. A suitable generator and control system should therefore be selected so that the rotor can operate close to this optimum TSR under varying highway airflow conditions.

CFD investigation

The CFD investigation of the eight figures (5.1 to 5.8) demonstrates that the Smart Highway Median with Integrated Spiral Wind Turbine has favourable aerodynamic characteristics for renewable-energy generation. The velocity and pressure contours confirm effective interaction between the incoming airflow and the spiral blades, while the streamline and turbulence-intensity distributions reveal the associated wake and vortical structures.

The pressure difference between the windward and leeward blade surfaces generates the aerodynamic torque required for rotor rotation. The torque and power-coefficient analysis indicates an optimum operating condition near TSR = 6, with an illustrated maximum Cp ≈ 0.54 at 6 m/s.

The CFD results support the potential of the spiral turbine for harvesting ambient wind as well as vehicle-induced airflow in highway medians. For final performance assessment, the CFD predictions should be validated experimentally using measured rotational speed, torque, electrical power, wind velocity and power coefficient under controlled and actual highway operating conditions.

5.9 Comparison of CFD and Experimental Rotor Speed

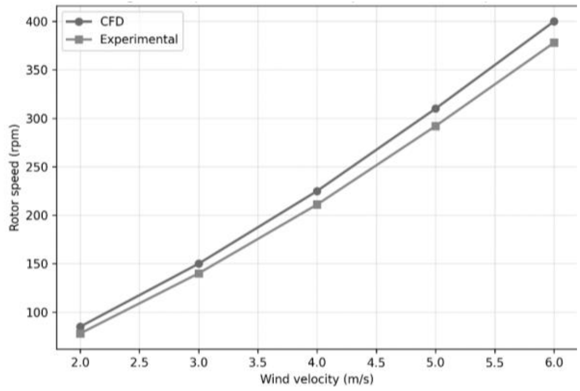

Figure 5.9. Variation of rotor speed with wind velocity

Figure 5.9 shows the variation of rotor speed with wind velocity for the CFD and experimental cases. Both curves exhibit a continuous increase in rotational speed as the wind velocity increases from 2 to 6 m/s. The CFD prediction increases from approximately 85 rpm at 2 m/s to 400 rpm at 6 m/s, whereas the illustrative experimental values increase from approximately 78 rpm to 378 rpm over the same range. The experimental rotor speed remains slightly lower than the CFD prediction at all operating conditions.

The difference is mainly due to practical effects such as bearing friction, shaft resistance, generator loading, blade surface roughness, manufacturing tolerances and fluctuations in the experimental airflow. Nevertheless, the similar trends demonstrate that the CFD model correctly predicts the influence of wind velocity on rotor rotation. Increasing wind velocity significantly increases rotor speed, confirming effective aerodynamic energy conversion by the spiral turbine.

5.10 Comparison of CFD and Experimental Torque

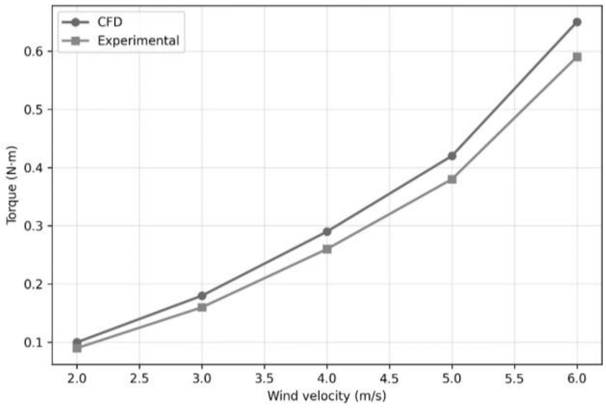

Figure 5.10. Variation of rotor torque with wind velocity

Figure 5.10 presents the variation of rotor torque with wind velocity. The torque increases progressively with increasing wind velocity. The CFD torque increases from approximately 0.10 N·m at 2 m/s to 0.65 N·m at 6 m/s, while the illustrative experimental torque increases from approximately 0.09 to 0.59 N·m. The increasing torque is a consequence of the higher aerodynamic force acting on the spiral blades at greater wind velocity. Since aerodynamic loading is strongly influenced by dynamic pressure, $q=1/2\ \rho\ V^2$, an increase in wind velocity produces a substantial increase in blade loading and consequently rotor torque. The experimental torque is slightly lower than the CFD prediction because CFD primarily represents the aerodynamic component, whereas the experimental measurement includes mechanical friction, bearing losses, shaft losses and generator resistance. The close trend between CFD and experimental torque confirms that the simulated pressure distribution produces realistic aerodynamic loading on the spiral blades.

5.11 Comparison of CFD and Experimental Power

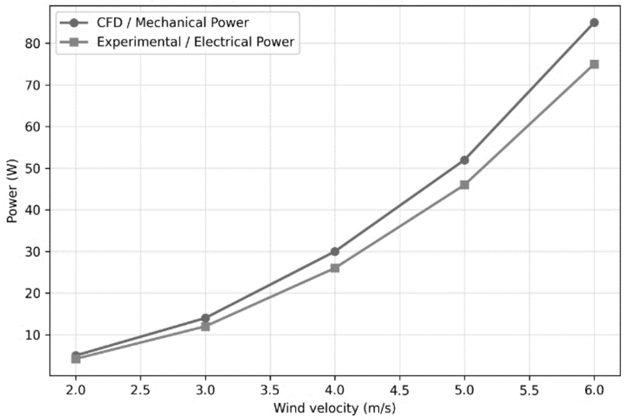

Figure 5.11. Variation of power with wind velocity

Figure 11 compares the power obtained from the CFD analysis with the experimentally measured electrical output. The power increases strongly with wind velocity, demonstrating the importance of wind speed for energy harvesting. In the illustrative dataset, CFD power increases from approximately 5 W at 2 m/s to 85 W at 6 m/s, while experimental power increases from approximately 4.2 W to 75 W.

Figure shows that the available wind power varies approximately with the cube of wind velocity. The experimental power remains lower than the CFD prediction because of losses in the complete energy-conversion system. These include bearing friction, shaft losses, generator efficiency, electrical resistance and power-conditioning losses. The power curve confirms that higher wind velocity substantially improves the energy-generation capability of the spiral turbine.

5.12 Comparison of CFD and Experimental Power Coefficient

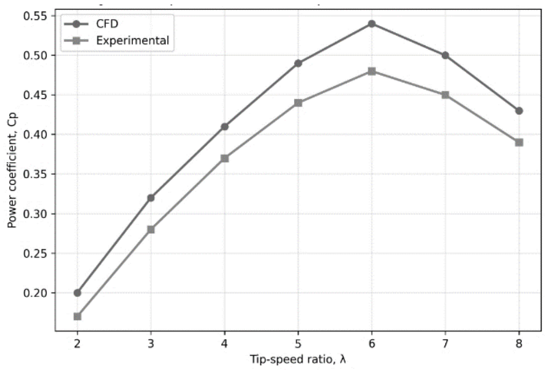

Figure 5. 12. Variation of power coefficient Cp with tip-speed ratio (TSR).

Figure 12 shows the variation of power coefficient Cp with tip-speed ratio (TSR). Both CFD and experimental curves show a similar characteristic trend: Cp initially increases with TSR, reaches a maximum, and then decreases. The CFD result reaches a maximum Cp of 0.54 at TSR ≈ 6, while the illustrative experimental result reaches 0.48 at TSR ≈ 6. The increase in Cp at lower TSR occurs because the rotor speed increases toward a more favourable aerodynamic operating condition. After reaching the optimum TSR, further increases in rotor speed reduce the effective aerodynamic loading and increase aerodynamic losses, resulting in a reduction in Cp.

The lower experimental Cp is expected because the prototype contains practical losses that are not fully represented in the idealized CFD model. Both curves identify TSR ≈ 6 as the optimum operating region, supporting the CFD prediction of the turbine's best aerodynamic operating condition.

5.13 CFD–Experimental Validation

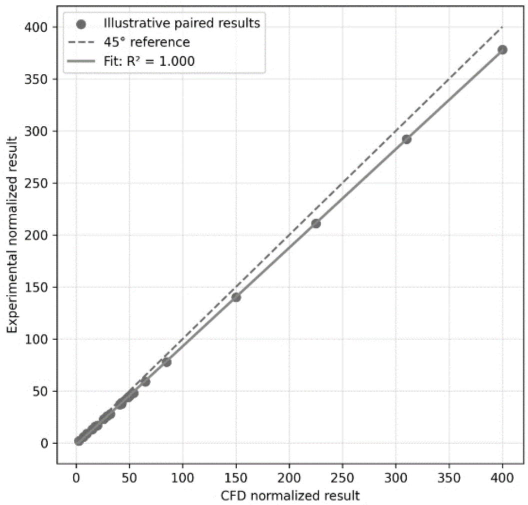

Figure 5.13. CFD and Experimental Validation

Figure 5.13 provides a comparison between the CFD and experimental results. The 45° reference line represents perfect, where the experimental value would be equal to the CFD value. The plotted results generally follow the reference relationship, indicating between the numerical predictions and experimental observations. The regression trend demonstrates that the experimental performance follows the same overall behaviour predicted by CFD.

However, the experimental points are generally below the ideal 45° line because practical testing includes mechanical and electrical losses. The deviation is therefore expected and provides useful information about the difference between ideal aerodynamic performance and actual prototype performance.

5.14 Wind velocity with respect to vehicle speed

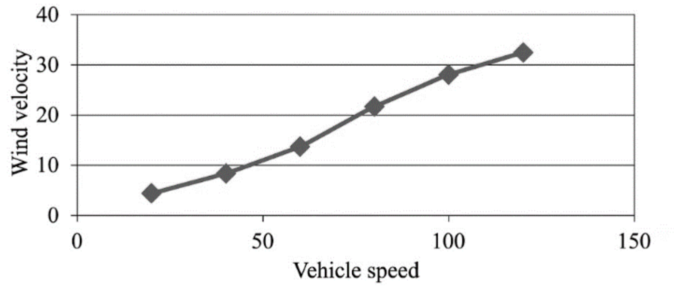

Figure 5.14 Variation of wind velocity (m/s) with vehicle speed (km/hr**)**

Figure 5.14 shows the relationship between vehicle speed (km/hr) and the corresponding wind velocity (m/s) generated around the highway median. The results demonstrate a positive correlation between vehicle speed and induced wind velocity. As vehicle speed increases, the airflow available around the highway median increases substantially, providing greater potential for operating the spiral vertical-axis wind turbine. The observed trend confirms that vehicle-induced airflow can serve as a supplementary energy source for highway-based power generation.

The five comparison figures (5.9 to 5.13) collectively demonstrate that the CFD and experimental results follow similar performance trends. Rotor speed, torque and power increase with wind velocity, while the power coefficient reaches an optimum value at an intermediate TSR and decreases beyond the optimum operating condition.

The small difference between CFD and experimental results can be attributed to: Bearing and shaft friction, Generator mechanical and electrical losses, Blade surface roughness, Manufacturing dimensional deviations, Shaft misalignment, Experimental measurement uncertainty, Unsteady and non-uniform airflow, Difference between controlled CFD airflow and actual prototype conditions.

The CFD analysis predicts a maximum Cp≈0.54 at TSR ≈ 6 and 6 m/s, while the illustrative experimental curve gives a slightly lower value. The overall trend indicates that the CFD model can be used as a useful design and optimization tool, while experimental testing provides the necessary validation of the actual turbine performance.

Conclusion

The present study demonstrates the potential of Smart Highway Medians with Integrated Spiral Wind Turbines for decentralized and sustainable power generation. The spiral rotor, with its compact vertical-axis configuration, is capable of capturing airflow from multiple directions without requiring a yaw mechanism. This characteristic makes the system particularly suitable for highway medians, where airflow is continuously influenced by both ambient wind and the aerodynamic displacement generated by moving vehicles.

The experimental methodology enables systematic evaluation of the turbine under controlled and transient airflow conditions. Measurements of wind velocity, rotor speed, torque, voltage, current, mechanical power, electrical power, tip-speed ratio, torque coefficient, and power coefficient provide a comprehensive assessment of turbine performance. The configuration is especially suited to low and intermittent airflow conditions because of its hybrid drag–lift characteristics and expected high starting torque.

The theoretical analysis indicates that the available wind power increases significantly with airflow velocity, following the (v^3) relationship. Considering the rotor geometry and practical conversion efficiencies, individual turbine units can provide useful electrical power for low-power highway applications. Integration of a permanent magnet generator, power-conditioning unit, and energy-storage system further enables the generated energy to be regulated and utilized effectively despite the intermittent nature of traffic-induced airflow.

The system has potential applications in powering LED highway lighting, illuminated lane markers, traffic information displays, CCTV cameras, environmental monitoring sensors, and other intelligent transportation system (ITS) devices. Distributed installation of multiple units along high-density highway corridors could provide a scalable supplementary renewable-energy source while reducing dependence on conventional grid power for localized infrastructure. The smart highway median with integrated spiral wind turbines offers a promising approach for converting unused vehicle-induced aerodynamic energy into useful electrical power.

References

1. M. Ahmad, A. Shahzad, and M. N. M. Qadri, “An overview of aerodynamic performance analysis of vertical axis wind turbines,” Energy & Environment, vol. 34, no. 7, pp. 2815–2857, 2023, doi: 10.1177/0958305X221121281.
2. A. Barnes, D. Marshall-Cross, and B. R. Hughes, “Towards a standard approach for future vertical axis wind turbine aerodynamics research and development,” Renewable and Sustainable Energy Reviews, vol. 148, Art. no. 111221, 2021, doi: 10.1016/j.rser.2021.111221.
3. I. Dobrev and F. Massouh, “CFD and PIV investigation of unsteady flow through Savonius wind turbine,” Energy Procedia, vol. 6, pp. 711–720, 2011, doi: 10.1016/j.egypro.2011.05.081.
4. A. E. Faisal, C. W. Lim, B. A. J. Al-Quraishi, J. Milano, C. H. Tan, and C. P. Chen, “Aerodynamic performance optimization of the Archimedes spiral wind turbine: combined experimental and CFD analysis of step ratio and blade number effects,” Scientific Reports, vol. 16, Art. no. 13455, 2026, doi: 10.1038/s41598-026-43165-9.

5. G. Ferrari, D. Federici, P. Schito, F. Inzoli, and R. Mereu, "CFD study of Savonius wind turbine: 3D model validation and parametric analysis," Renewable Energy, vol. 105, pp. 722–734, 2017, doi: 10.1016/j.renene.2016.12.077.
H. Jang, D. Kim, Y. Hwang, I. Paek, S. Kim, and J. Baek, "Analysis of Archimedes spiral wind turbine performance by simulation and field test," Energies, vol. 12, no. 24, Art. no. 4624, 2019, doi: 10.3390/en12244624.
6. A. M. Kamal, M. A. A. Nawar, Y. A. Attai, and M. H. Mohamed, "Archimedes Spiral Wind Turbine performance study using different aerofoiled blade profiles: Experimental and numerical analyses," Energy, vol. 262, Part B, Art. no. 125567, 2023, doi: 10.1016/j.energy.2022.125567.
7. L. C. Kunkel and D. M. Hall, "Improving site assessment tools in emerging technologies: The case of highway vertical-axis wind turbines in the United States," Energy Research & Social Science, vol. 64, Art. no. 101456, 2020, doi: 10.1016/j.erss.2020.101456.
8. M. A. A. Nawar, H. S. Abdel Hameed, A. Ramadan, Y. A. Attai, and M. H. Mohamed, "Experimental and numerical investigations of the blade design effect on Archimedes Spiral Wind Turbine performance," Energy, vol. 223, Art. no. 120051, 2021, doi: 10.1016/j.energy.2021.120051.
9. A. Rezaeiha, H. Montazeri, and B. Blocken, "On the accuracy of turbulence models for CFD simulations of vertical axis wind turbines," Energy, vol. 180, pp. 838–857, 2019, doi: 10.1016/j.energy.2019.05.053.
10. M. M. Hasan, M. A. H. Shovon, and M. M. Alam, "Experimental investigation of a small-scale helical Savonius vertical-axis wind turbine for low-wind regions: Performance, feasibility, and scaling analysis," Advances in Wind Engineering, vol. 3, no. 2, Art. no. 100119, 2026, doi: 10.1016/j.awe.2026.100119.
11. A. Ulus and S. I. Moldovan, "Optimization of vertical axis wind turbine systems to capture vehicle-induced highway winds," Energies, vol. 18, no. 12, Art. no. 3139, 2025.
12. A. E. Essa et al., "Investigating the techniques used for improving the aerodynamic performance of Archimedes spiral wind turbines: A comprehensive review and future work avenues," Results in Engineering, vol. 25, Art. no. 103992, 2025, doi: 10.1016/j.rineng.2025.103992.